Ocean Engineering 266 (2022) 112692

Contents lists available at ScienceDirect

Ocean Engineering

journal homepage: www.elsevier.com/locate/oceaneng

A new FounDyn module in OpenFAST to consider foundation dynamics of monopile supported wind turbines using a site-specific soil reaction framework

Lilin Wang [a,b,*], Takeshi Ishihara [b]

[a] Ocean College, Zhejiang University, Zhoushan, 316021, PR China
[b] Department of Civil Engineering, School of Engineering, The University of Tokyo, 7-3-1, Hongo, Bunkyo-ku, Tokyo, Japan

ARTICLE INFO

Keywords:
Wind turbine
Monopile
FounDyn module
Site-specific soil reaction
Earthquake

ABSTRACT

A FounDyn module is created in OpenFAST to consider foundation dynamics, which is an appealing supplement to the current version of OpenFAST. The FounDyn module receives the motions from the SubDyn module and sends the forces back to the SubDyn module. In FounDyn, the soil-monopile interaction is captured using a site-specific soil reaction framework. The soil reaction framework possesses the same configuration of the semi-analytical 1D model to consider effects of the large plie diameter and the small pile aspect ratio but uses new site-specific soil reaction models. The soil reaction models are nonlinear and hysteretic, which match the desired modulus reduction curve by identifying three parameters in a hyperbolic function and a linear function using genetic algorithm (GA) and manual parameter tuning, and the desired damping curve by applying the Ishihara-Yoshida rule that controls the unloading-reloading curves iteratively through three parameters. The FounDyn module is verified by the well-confined OC3 project in terms of modal frequencies, tower top displacement and shear force and moment at the mudline, and reasonable agreements are achieved between them. A series of emergency shutdown analyses of the NREL 5 MW wind turbine are performed using OpenFAST plus FounDyn. The results show that the misalignment of wind and earthquake affects the tower bending moments largely. The earthquake excitation is found to be the design driving load, prevailing over the wind excitation for the design of wind turbine supporting structures.

1. Introduction

Offshore wind turbines are complicated systems that consist of rotor nacelle assembly (RNA), control system, tower, substructure, and foundation, which suffer from environmental loads such as wind, wave, earthquake, etc. The dynamic responses of offshore wind turbines are coupled with the external environmental conditions, foundation dynamics, and intelligent control algorithms, which means the interactions among them shall be not neglected. As a popular simulation tool of offshore wind turbines, FAST can model the RNA and tower well, and the environmental loads are well considered in it. However, a fixed foundation is used in FAST till this study was performed, which makes it unable to consider the soil-structure interaction accurately (Jonkman and Buhl, 2005).

Several pieces of research have been conducted to achieve the integrated analysis of offshore wind turbines by modifying the open-source software FAST. Jung et al. (2015) developed a macro-spring model in FAST to consider the soil-pile interaction, that is, a concentrated nonlinear elastic soil spring was set at the mudline to achieve a simplified soil-pile interaction simulation. Similarly, Krathe and Kaynia (2017) also developed a macro-spring model at the mudline in FAST to further consider the nonlinear hysteresis characteristics of soil-pile interaction, so that the damping effect of the soil-pile interaction can be reflected. In addition, Loken and Kaynia (2019) also proposed an integrated model for the analyses of offshore wind turbines based on the modification of FAST. In their model, the foundation that is originally fixed at the mudline was expanded to a certain depth below the mudline to mimic the stiffness of soil-pile interaction. A decrease in modal frequencies of offshore wind turbines can be realized by the flexibility of the extended cantilever beam. However, this method cannot reflect the real condition of the pile base. In summary, the soil-pile interaction was considered somehow in the above-mentioned researches. However,

* Corresponding author. Ocean College, Zhejiang University, Zhoushan, 316021, PR China.
E-mail address: lilin.wang@zju.edu.cn (L. Wang).

https://doi.org/10.1016/j.oceaneng.2022.112692
Received 3 March 2022; Received in revised form 21 September 2022; Accepted 22 September 2022
Available online 17 October 2022

these considerations of soil-pile interactions are too simplified to predict the dynamic responses of monopiles accurately.

Several pieces of research were performed to implement the foundation dynamics and earthquake excitations in FAST. Prowell (2011) implemented an advanced seismic module in FAST V7. The module can specify a platform motion time series as displacement, velocity, or acceleration independently in the X, Y, and Z axes. The force required to achieve the desired motion is calculated at run time for each time step and applied to the wind turbine platform in FAST using a damped oscillator model. However, their implementation did not directly support the consideration of base rocking, twisting, or soil-structure interaction (SSI). Yang et al. (2020) implemented a seismic analysis framework (SAF) in FAST V7. Although they stated the shortcomings of the API p-y curve, it was used to model the soil-pile interaction for the seismic analysis in their study. All previous researchers implemented their methods in FAST V7 using a user-specified subroutine UserPtfmLd. However, no pieces of research focus on the widely-used version of FAST, OpenFAST.

Previous dynamic analyses of offshore wind turbines were performed with fixed foundations, in which the soil-pile interactions are not considered (Wei et al., 2013; Kim et al., 2016). Thus, it is needed to review the influence of soil-pile interaction on the dynamic loadings of wind turbine supporting structures. Bush and Manuel (2009) studied the dynamic responses of an offshore wind turbine supported by the monopile and the sandy seabed. Compared to the fixed foundation, the peak value and the cyclic amplitude of bending moment at the mudline will increase by 15% and 20%, respectively if the soil-pile interaction is considered. Similar conclusions were reported by Krathe (2015). Jung et al. (2015) modelled the soil-pile interaction using the macro-spring model and found that the soil-pile interaction affects not only the dynamic responses but also the modal properties of offshore wind turbines. The natural frequency of the wind turbine will be overestimated by 14% if the soil-pile interaction is not considered. Loken and Kaynia (2019) also found that when the soil-pile interaction is considered, the maximum bending moment at the mudline increased by 1%, while the cyclic amplitude of the bending moment increased by 7%. The peak value relates to the ultimate bearing capacity of the wind turbine supporting structure, while the cyclic amplitude affects the fatigue life of the wind turbine supporting structure. A 7% increase in the cyclic amplitude of the bending moment would increase fatigue damage by 28% since an offshore wind turbine is subjected to millions of cyclic loads during its 25-year service life. To summarize, if the fixed foundation is used, the cyclic amplitude of the dynamic loading will be underestimated, and the fatigue life of the monopile will be overestimated, which leads to an unsafe design. Since the above results are based on simple soil-structure interaction models, the accuracy and reliability need to be further evaluated. Regarding the seismic consideration in the design of wind turbines, many studies were conducted in the past decades (Wang and Ishihara, 2020). However, most researchers tend to use the finite element models instead of the aero-elastic models since the earthquake excitation and foundation dynamics are not well addressed in the wind turbine simulation software, such as OpenFAST. Compared to the aero-elastic model, an obvious shortcoming of the finite element model is that it cannot consider the rotor dynamics and the servo dynamics.

In this study, the integrated dynamic analyses of offshore wind turbines are performed by creating a new FounDyn module in OpenFAST to consider the foundation dynamics of offshore wind turbines. The outline of this paper is given as follows: a site-specific soil reaction framework for monopiles is updated and a FounDyn module is created in OpenFAST in Section 2. The FounDyn module is verified and demonstrated in Section 3. The application of OpenFAST plus FounDyn to the integrated dynamic analysis of a monopile-supported wind turbine is demonstrated in Section 4. Conclusions are given in Section 5.

2. A new FounDyn module in OpenFAST with a site-specific soil reaction framework

2.1. A site-specific soil reaction framework for soil-monopile interaction

Wang and Ishihara (2022) proposed a semi-analytical one-dimensional (1D) model for the soil-structure interaction of pile foundations under the combined lateral, vertical, and torsional forces. The reason why the model is semi-analytical is that a correction factor κ (see Eq. (A1)) is introduced in the calculation of ultimate capacities of lateral and rotational soil reactions and fitted based on three-dimensional finite element analyses. However, the soil reactions in the proposed model use empirical models (PySimple1, TzSimple1, etc.) that were fitted to the test results of certain soil conditions. The applicability of these soil reactions to soil conditions other than those examined is uncertain (Zhang et al., 2021; Lai et al., 2021). To improve the applicability of the proposed model, a site-specific soil reaction framework is formed using the same configuration of the semi-analytical 1D model, but with site-specific soil reactions. Since a site-specific p-y model PySimple5 has been proposed by the author (Wang and Ishihara, 2022a,b), other site-specific soil reactions ($S_{y,\mathrm{pb}} - v_{y,\mathrm{pb}}$, $m_x - \theta_x$, $m_{x,\mathrm{pb}} - \theta_{x,\mathrm{pb}}$, $t_z - v_z$, $Q_{z,\mathrm{pb}} - v_{z,\mathrm{pb}}$) can be proposed using the same ideas. More specifically, these site-specific soil reactions shall match the desired modulus reduction curve by identifying three parameters in a hyperbolic function and a linear function using the genetic algorithm (GA) and manual parameter tuning algorithm, and the desired damping curve by applying the Ishihara-Yoshida rule that controls the unloading-reloading curves iteratively through three parameters. It should be noted that the proposal of site-specific soil reactions is not the focus of this paper, the originality of this study exists that the author tends to implement this advanced soil reaction framework in the widely-used aero-elastic software OpenFAST to support the integrated analysis of monopile supported wind turbines. According to the author's knowledge, this meaningful research has not been investigated in previous studies.

Fig. 1 illustrates the procedure to propose the configuration of the site-specific soil reaction framework (same as the semi-analytical 1D model). Fig. 1(a) presents the monopile with the external excitations. Fig. 1(b) shows the stress distribution on the monopile from the soil. Fig. 1(c) shows the fishbone-shaped model for the monopile, from which the configuration of the site-specific soil reaction framework can be derived as shown in Fig. 1(d). The site-specific soil reaction framework includes the lateral, rotational and vertical soil reactions along the pile shaft and at the pile base. More details about Fig. 1a-d can be found in Wang and Ishihara (2022a). The site-specific soil reactions in the proposed model are summarized in Table 1. MθSimple5 is selected to demonstrate the idea of site-specific soil reactions since few pieces of research focused on the rotational soil reaction.

Following the idea of PySimple5, MθSimple5 is proposed to consider the coupling between axial and lateral resistances. Following the Japanese guideline for the seismic soil-pile interaction analysis, the modulus reduction and damping curves shall be matched in the proposed soil reaction curve (Ishihara, 2010). MθSimple5 adopts the linear ($M^e - \theta^e$) and hyperbolic ($M^p - \theta^p$) components in series. The governing equations of MθSimple5 are expressed in Eqs. (1)–(7). The force and stiffness in the linear component (Eqs. (1) and (2)), in the hyperbolic component (Eqs. (3) and (4)), and the overall spring (Eqs. (5) and (6)) are presented herein briefly. Eq. (7) defines the yield function used in MθSimple5. Note that Eq. (3) shows that the unloading and reloading are achieved by updating the reversal point (θ_0^p, m_0) in the plastic component of MθSimple5, which is different from the widely-used Masing rule. Parameters in MθSimple5 can be divided into backbone curve relevant parameters (c, n, η), unloading-reloading relevant parameters (A, B, E), soil properties relevant parameters (m_{ult}, $h_{\max}$, θ_{50}) and others (m_0, θ_0^p, m_0^d, θ_0^g, θ_0^+, θ_0^-).

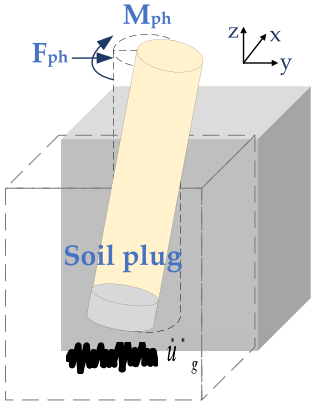

(a) Monopile with seismic excitation

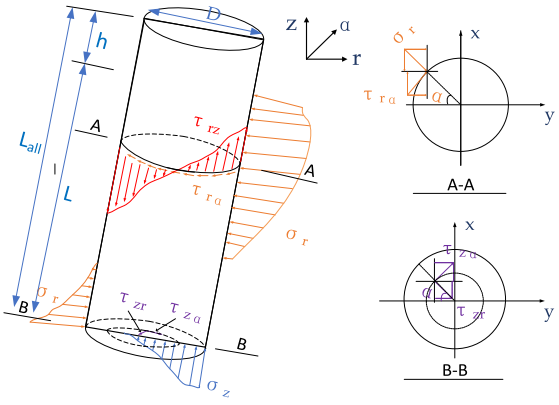

(b) Indication of stress on monopile from soil

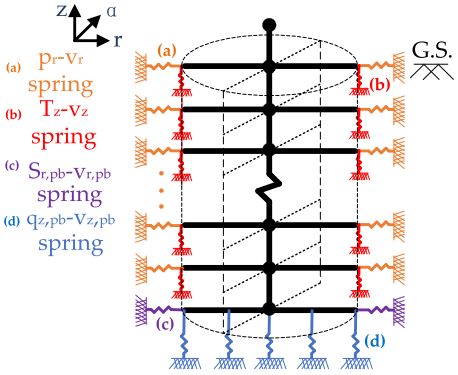

(c) Fishbone frame model (4 types of springs)

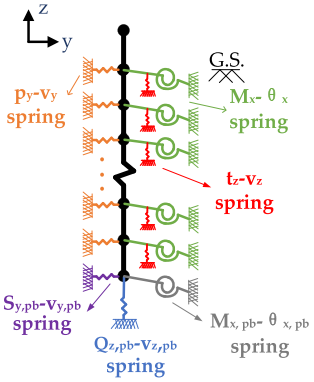

(d) Semi-analytical 1D model

Fig. 1. Monopile foundation and its dynamic semi-analytical model.

Table 1
Soil reaction models in the Semi-analytical 1D model for monopiles.

Spring name	Soil reaction component	Soil reaction curves
$p_y - v_y$	Lateral for pile shaft	PySimple5
$S_{y,pb} - v_{y,pb}$	Lateral for pile base	TzSimple5
$m_x - \theta_x$	Rotational for pile shaft	MθSimple5
$m_{x,pb} - \theta_{x,pb}$	Rotational for pile base	MθSimple5
$t_z - v_z$	Vertical for pile shaft	TzSimple5
$Q_{z,pb} - v_{z,pb}$	Vertical for pile base	QzSimple5

$$M^e = K^e \theta^e \tag{1}$$

$$K^e = \eta \frac{m_{ult}}{\theta_{50}} \tag{2}$$

$$m^p = B \cdot E \cdot m_{ult} - (B \cdot E \cdot m_{ult} - m_0)\left(\frac{A \cdot E \cdot c \cdot \theta_{50}}{A \cdot E \cdot c \cdot \theta_{50} + |\theta^p - \theta_0^p|}\right)^n \tag{3}$$

$$K^p = \frac{\partial m^p}{\partial \theta^p} = \frac{n \cdot sign(\dot{y})(B \cdot E \cdot m_{ult} - m_0)}{|\theta^p - \theta_0^p| + A \cdot E \cdot c \cdot \theta_{50}}\left[\left(\frac{A \cdot E \cdot c \cdot \theta_{50}}{|\theta^p - \theta_0^p| + A \cdot E \cdot c \cdot \theta_{50}}\right)^n\right] \tag{4}$$

$$m = m^e = m^p \tag{5}$$

$$K = (1/K^e + 1/K^p)^{-1} \tag{6}$$

$$f = |m - m_\alpha| - (C_r \cdot m_{ult}) \tag{7}$$

where K^e is the elastic modulus, K^p is the plastic modulus, and K is the combined modulus. f is the yield function; m_α is the value of m at the center of the elastic region (analogous to the backstress in the classical plasticity theory), $C_r \cdot m_{ult}$ is the yielding force and C_r is 0 in Pysimple5, m_0 is the value of m at the start of current plastic loading cycle and m_{ult} is the ultimate bearing capacity. θ^e is the elastic component of displacement, θ^p is the plastic component of displacement, θ_0^p is the value of θ_0 at the start of current plastic loading cycle and θ_{50} is the displacement where $m = 0.5m_{ult}$. θ_0^+ is the memory term for the positive side of the gap, θ_0^- is the memory term for the negative side of the gap. The initial values of θ_0^+ and θ_0^- are $\theta_{50}/100$ and $-\theta_{50}/100$, respectively. Stiffness constants c, n, η define the shape of the backbone curve of the MθSimple5.

The backbone curve relevant parameters (c, n, η) can be identified by GA using the criterion that the backbone curve shall be capable of matching the desired modulus reduction curve. The fitness function of GA, $1/RMSE$, is defined as the ratio of root mean squared error in Eq. (8), while the iteration will be stopped when Eq. (9) is satisfied or the generation reaches 100. Note that the results of GA may be not stable and manual parameter tuning algorithm can be used to determine the final values of c, n, and η.

$$RMSE = \sqrt{\frac{1}{N}\sum_{i=1}^{N}\left(\frac{K_i}{K_0} - \frac{G_i}{G_0}\right)^2} \tag{8}$$

$$RMSE \le 10^{-3} \text{ or } \varphi_j - \varphi_{j-1} \le 10^{-3} \tag{9}$$

where $RMSE$ means the root mean square error. G_i is the modulus at the ith points of the modulus reduction curve, while K_i is the corresponding stiffness of the p-y curve. N is the number of points on the modulus reduction curve used for identification, which could be 10–20 uniformly distributed points on the modulus reduction curve. G_0 and K_0 are the initial shear modulus and stiffness, respectively. φ_j means the parameter at the jth generation and φ could be c, n, or η.

The site-specific modulus reduction and damping curves can be described by the well-organized Hardin-Drnevich model (Hardin and Drnevich, 1972). One example of identified parameters is given in Table 1 by fitting to $G/G_0 = 1/(1+\gamma/\gamma_{0.5})$ with $\gamma_{0.5} = 0.25\%$ in the Hardin-Drnevich model. The backbone curve and corresponding modulus reduction curve using the parameters in Table 2 are portrayed in Fig. 2. It is observed that the proposed model can match well with the desired modulus reduction curve. The relationship between displacement (θ) and strain (γ) proposed by Lai et al. (2021) is used to convert displacement into strain ($\theta = 0.8\gamma$) and guarantees that $K/K_0 = 1/(1+\theta/\theta_{50})$ and $h = h_{\max}\theta/(\theta_{50}+\theta)$ for the p-y curve corresponds to $G/G_0 = 1/(1+\gamma/\gamma_{0.5})$ and $h = h_{\max}\gamma/(\gamma_{0.5}+\gamma)$ for the Hardin-Drnevich model.

The unloading-reloading relevant parameters (A, B, E) can be updated using the Ishihara-Yoshida rule (Ishihara et al., 1985) following the criterion that the backbone curve shall be capable of matching the damping curve. The Ishihara-Yoshida rule was proposed for ground response analyses to solve the overestimation of soil damping when the soil strain is large. The same idea is used in this study for p-y modeling. A, B and E have different values for different loading conditions as shown in Eq. (10) and are obtained iteratively to match the damping curve using Eqs. (11)–(13). It is noted that Eqs. (12) and (13) cannot be solved in a closed form for a_0 and e_0. They are solved numerically using the bisection method. The iteration will be stopped when Eq. (14) is satisfied. Eq. (5) is also examined, and the iteration will be stopped when Eq. (15) is satisfied or the number of iterations reaches 20. Fig. 3 compares the hysteresis loops and damping curves with and without the Ishihara-Yoshida rule. It is noticed that the damping at large strains will be significantly overestimated without using the Ishihara-Yoshida rule to modify the hysteresis loop.

$$\begin{cases} \text{skeleton curve: } A = 1, B = 1, E = 1 \\ \text{unloading: } A = a_0, \quad B = b_0, \quad E = 1 \\ \text{reloading \& reunloading: } A = a_0, \quad B = b_0, \quad E = e_0 \end{cases} \tag{10}$$

$$b_0 = \frac{\left(\frac{c\cdot\theta_{50}}{c\cdot\theta_{50}+\left|\theta_0^p\right|}\right)^n - 1}{\left(\frac{a_0\cdot c\cdot\theta_{50}}{a_0\cdot c\cdot\theta_{50}+\left|\theta_0^p\right|}\right)^n - 1} \tag{11}$$

$$D\left(\frac{\theta_{0i}^p}{a_0}\right) = h(\theta_{0i}^p) \tag{12}$$

$$f\left(\frac{y_{0i}^p}{a_0}\right) = \frac{p_{0i}/b_0}{e_0} \tag{13}$$

Here, $h(\theta) = h_{\max}\left(\frac{\theta}{\theta_{50}+\theta}\right)$, $D(\theta) = \frac{1}{4\pi}\frac{\Delta W(\theta)}{W(\theta)}$, $W(\theta) = \frac{1}{2}\theta\cdot g(\theta)$, $\Delta W(\theta) = 2\int_{-\theta}^{\theta} g(\theta_0)d\theta_0$,

Table 2
One example of identified parameters for the modulus reduction curve in the H-D model.

Soil condition	Material constants	M0Simple5
Clay or Sand	c	0.5
	n	0.7
	η	3.5

$$g(\theta) = \begin{cases} m_{ult} - (m_{ult} - m_{0i}/b_0)\left(\frac{c\cdot\theta_{50}}{c\cdot\theta_{50}+(\theta-\theta_{0i}^p/a_0)}\right)^n & (\Delta\theta > 0) \\ -m_{ult} + (m_{ult} + m_{0i}/b_0)\left(\frac{c\cdot\theta_{50}}{c\cdot\theta_{50}-(\theta-\theta_{0i}^p/a_0)}\right)^n & (\Delta\theta < 0) \end{cases}$$

$$f(\theta) = \begin{cases} m_{ult} - \left(m_{ult} - \frac{m_{0i+1}/b_0}{e_0}\right)\left(\frac{c\cdot\theta_{50}}{c\cdot\theta_{50}+\left(\frac{\theta-\theta_{0i+1}^p/a_0}{e_0}\right)}\right)^n & (\Delta\theta > 0) \\ -m_{ult} + \left(m_{ult} + \frac{m_{0i+1}/b_0}{e_0}\right)\left(\frac{c\cdot\theta_{50}}{c\cdot\theta_{50}-\left(\frac{\theta-\theta_{0i+1}^p/a_0}{e_0}\right)}\right)^n & (\Delta\theta < 0) \end{cases}$$

where $h(\theta)$ is the desired damping curve. $D(\theta)$ represents the damping corresponds to the p-y loops. $\Delta W(\theta)$ is the damping energy and $W(\theta)$ is the equivalent elastic strain energy. The coordinates (θ_{0i}^p, m_{0i}) and $(\theta_0^p i+1, m_{0i+1})$ are the most recent two reversal points.

$$\text{abs}\left(D\left(\frac{\theta_{0i}^p}{a_0}\right) - h(\theta_{0i}^p)\right) \Big/ h(\theta_{0i}^p) \le 1.0e^{-3} \text{ or abs}\left(D\left(\frac{\theta_{0i}^p}{a_0}\right) - h(\theta_{0i}^p)\right) \le 1.0e^{-3} \tag{14}$$

$$\frac{2m - m^e - m^p}{m_{\text{ult}}} \le 1.0e^{-12} \tag{15}$$

2.2. A new FounDyn module in OpenFAST

OpenFAST is a multi-physics, multi-fidelity tool for simulating the coupled dynamic response of wind turbines, which couples computational modules for aerodynamics, hydrodynamics for offshore structures, control, and electrical system (servo) dynamics, and structural dynamics to enable coupled nonlinear aero-hydro-servo-elastic simulation in the time domain. However, the foundation is the least considered in OpenFAST among the important components of wind turbines. Since more and more wind turbines are installed in seismically active regions, it is also necessary to supplement the foundation dynamics into OpenFAST for the seismic analysis of onshore and offshore wind turbines. In this study, a FounDyn module is created in OpenFAST to address the foundation dynamics. As given in Fig. 4, the newly implemented FounDyn module works similarly to the HydroDyn module when it is applied to an offshore wind turbine. That is, the FounDyn module first receives the motions from the SubDyn module and then sends back the forces and moments from the soil-structure interaction and seismic excitation to the SubDyn module at each time step. To achieve this, SubDyn module needs to be modified to remove the base fixity to incorporate the dynamics of a foundation, i.e., monopile. The configuration of OpenFAST with the FounDyn module is depicted in Fig. 5, in which the red color shows the new implementation of the FounDyn module in OpenFAST. Note that the seismic submodule in the FounDyn module uses the same method as that provided by Prowell (2011). The FounDyn module includes the SSI submodule and the earthquake submodule. The proposed semi-analytical 1D model is extended to the 3D model and implemented in the SSI submodule. Currently, a similar module called SoilDyn is implemented using constant spring stiffnesses and dashpot dampings to consider the soil-structure interaction for wind and wave dynamics in OpenFAST, which is also absorbed as part of the SSI submodule. Therefore, the FounDyn module can consider different SSI models and loading conditions including wind, wave, and earthquake.

3. Verification of the FounDyn module in OpenFAST

The FounDyn module is verified by the OC3 project. The International Energy Association (IEA) performed the Offshore Code Comparison Collaboration (OC3) project to investigate offshore wind technology and deployment. In the OC3 project, the NREL 5 MW wind

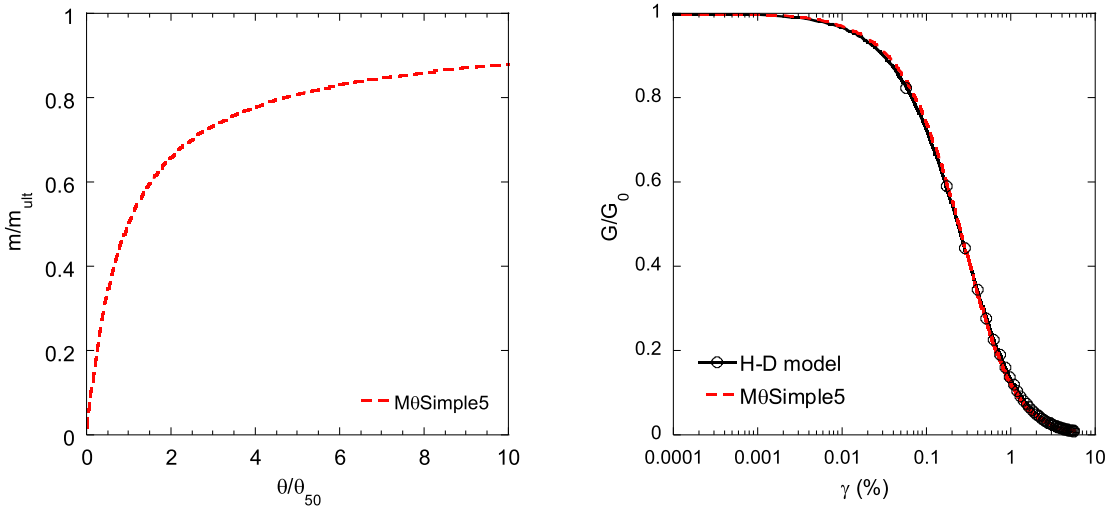

(a) Backbone curve (b) Modulus reduction curve

Fig. 2. One example of MθSimple5 backbone curve with parameters in Table 1 and modulus reduction curve derived from MθSimple5.

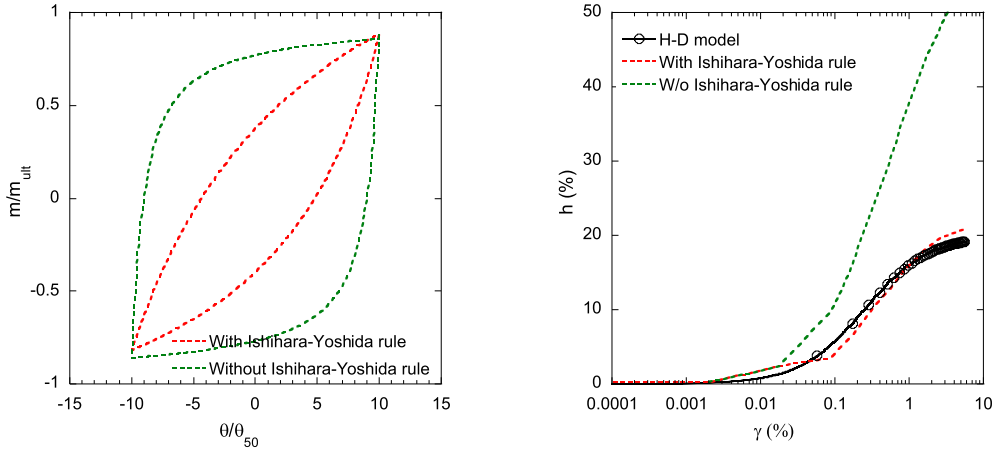

(a) Normalized hysteresis loops (b) Damping curves

Fig. 3. One example of MθSimple5 hysteresis loop and damping curve with and without Ishihara-Yoshida rule.

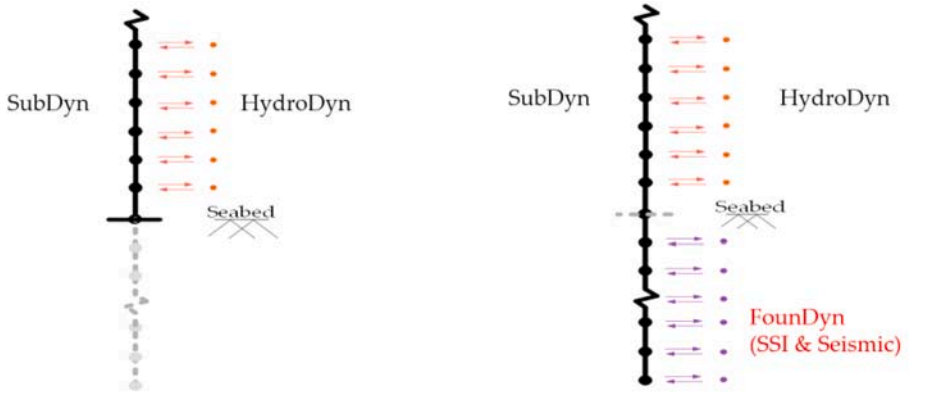

(a) Original SubDyn Module (b) Modified SubDyn Module

Fig. 4. Comparison of original and modified SubDyn modules.

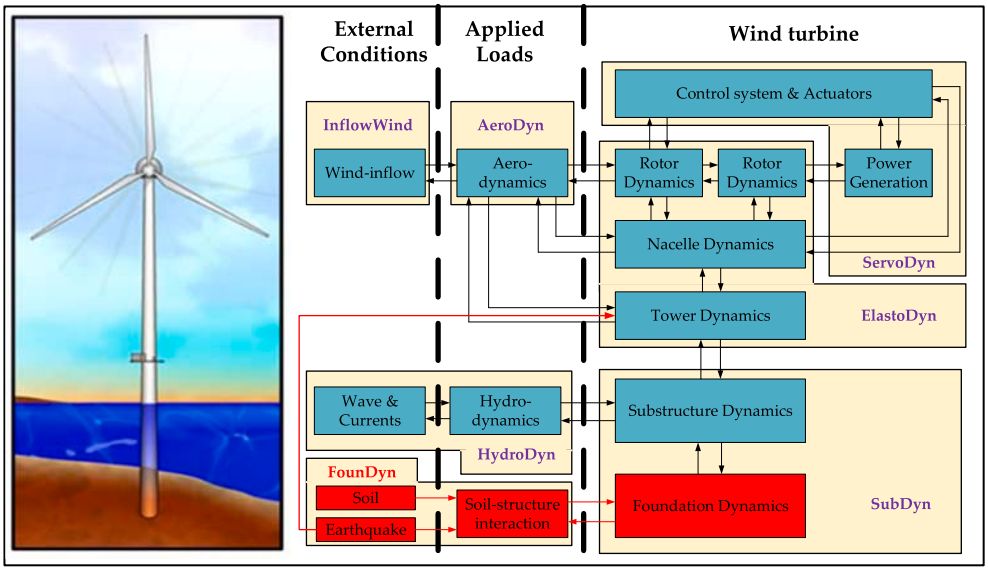

Fig. 5. Module configuration of OpenFAST with FounDyn.

turbine with a monopile foundation is studied. The diameter and thickness of monopile are 6m and 0.06m, respectively. The embedment of monopile is 36m. The information of the wind turbine is summarized in Table 3. The soil profile is shown in Fig. 6. For the OC3 project, Jonkman et al. (2008) and Jonkman and Musial (2010) simulated the wind turbine responses using the distributed linear springs to consider the soil-structure interaction. The spring stiffness is obtained by using the initial stiffness of API p-y curves. During their simulation, the wind speed of hub height is 11.4 m/s and the turbulent wind is generated using the Kaimal spectrum with a turbulent density of 14%. The wave is generated using the Jonswap spectrum with an effective wave height of 6m and a wave period of 10s.

To verify the FounDyn module, the parameters of the proposed model shall be consistent with those in Jonkman and Musial (2010). More specifically, the stiffnesses of rotational soil reactions for pile shaft and base shall be small enough to be negligible. Therefore, the proposed model is reduced to the p-y model. The initial stiffness of the p-y model shall be the same as that in Jonkman and Musial (2010). Note that there is an option used in the FounDyn to determine whether nonlinear soil reactions are considered. When the option is set as false, the initial stiffness is used to linearize soil reactions. Table 4 shows comparisons of simulation results between the FounDyn and the OC3 project (Jonkman et al., 2008). It is noticed that the predicted frequencies by the FounDyn agree well with those in the OC3 project. Table 5 illustrates the dynamic responses of the wind turbine predicted by the FounDyn and the OC3 project. The results show that the differences between the two methods

Table 3
Properties of the NREL 5 MW Baseline OWT with a monopile support structure.

Rating	5 MW
Rotor orientation, configuration	Upwind, 3 blades
Rotor diameter	126 m
Hub-height	90 m
Tower top diameter, wall thickness	3.87, 0.019 m
Tower base diameter, wall thickness	6.0, 0.027 m
Substructure diameter, wall thickness	6.0, 0.06 m
Cut-in, rated, cut-out wind speed	3, 11.4, 25 m/s
Rated rotor speed	12.1 rpm
Rated tip speed	80 m/s
Rotor mass	110,000 kg
Nacelle mass	240,000 kg
Tower mass	346,460 kg
Mean sea level	20.0m

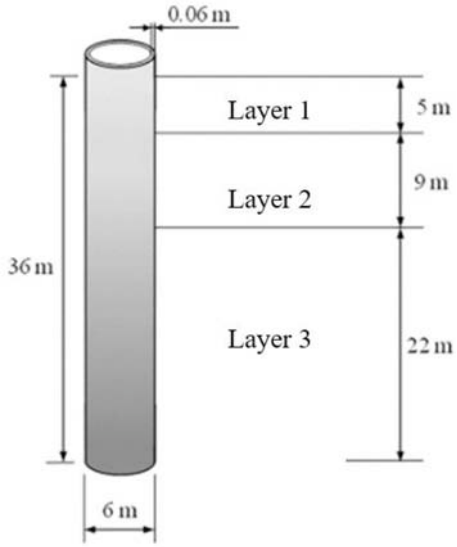

Fig. 6. The soil-monopile system in the IEA OC3 project.

Table 4
Comparison of predicted modal frequencies by the OC3 project and FounDyn.

Modal frequencies	FA 1st mode	SS 1st mode	FA 2nd mode	SS 2nd mode
OC3 project	0.248	0.246	1.546	1.533
FounDyn	0.245	0.240	1.530	1.494

Note:FA means the fore-aft direction , SS means the side-side direction.

are smaller than 5% in terms of the mean value, maximum value, and standard deviation of the tower top displacement, the shear force at the mudline, and the moment at the mudline. It means that the FounDyn module can predict the soil-structure interaction of monopiles accurately.

It is important to examine whether the proposed soil reaction model is implemented properly. To illustrate the nonlinearity of the proposed soil reaction model, a series of sinusoidal uniform wind flows are defined in Fig. 7 and applied to the above NREL 5 MW wind turbine. The amplitudes of sinusoidal uniform wind flows are set to mimic the realistic behavior of wind and the period is close to the natural period of the

Table 5
Comparison of predicted dynamic responses by the OC3 project and FounDyn.

Response	TTD (m)			$Q_{mudline}$ (MN)			$M_{mudline}$ (MNm)		
	Mean	Maximum	STD	Mean	Maximum	STD	Mean	Maximum	STD
OC3 project	0.509	0.931	0.113	0.409	4.053	1.099	57.502	124.800	20.198
FounDyn	0.510	0.925	0.111	0.407	4.041	1.085	57.050	122.621	19.848
Difference (%)	**0.196**	**0.644**	**1.770**	**0.489**	**0.296**	**1.274**	**0.786**	**1.746**	**1.733**

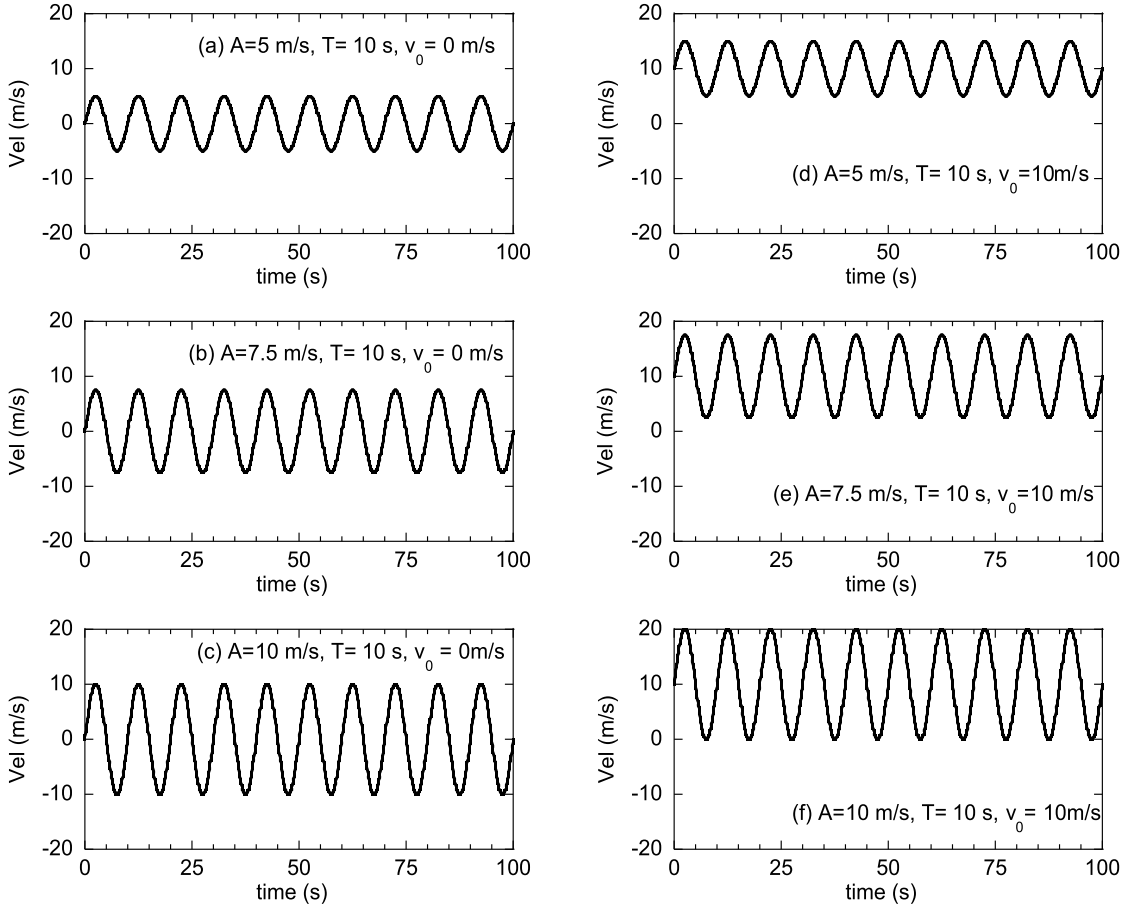

Fig. 7. Harmonic wind velocities.

turbine. During the simulation, the sinusoidal wind is the only excitation input, and others from the HydroDyn FounDyn modules are eliminated. The corresponding hysteretic responses for the $M_y - \theta_y$ spring at 1 m below the mudline are illustrated in Fig. 8. The hysteresis loops show that a nonlinear behavior is successfully implemented in the FounDyn module. Since the area under the loop represents soil damping, the larger loop means that the more soil damping exits. It is also observed that larger rotations and moments are observed for the cases with the mean velocity of 10 m/s than those with the mean velocity of 0 m/s.

4. Application of the FounDyn module for dynamic analyses of monopile-supported wind turbines under wind and earthquake

4.1. Configuration of numerical simulations

The IEC 61400-1 guideline suggests that the earthquake loading shall be superposed with operational loading that shall be equal to the higher of a) loads during normal power production by averaging over the lifetime; b) loads during the emergency shutdown for a wind speed selected so that the loads prior to the shutdown are equal to those obtained with a). To demonstrate the combination of earthquake loading and operational loading, a series of emergency shutdown analyses are performed with the parameters in Table 6. In Table 6, the wind flow is uniform and constant with a velocity of 11.4 m/s, while 15 earthquake waves are used to consider the phase characteristic and for each earthquake wave. The simulations are demonstrated using the NREL 5 MW wind turbine, whose information can be found in Section 3.1. The targeted wind turbine is assumed to be supported by a monopile embedded in a uniform sand layer. The information of monopile and supporting soil are given in Table 7 and Table 8, respectively. It is assumed that the nonlinearity of the supporting soil can be modelled using the Hardin-Drnevich model with parameters of $\gamma_{0.5} = 0.1\%$ and $h_{max} = 21\%$. In addition, the properties of the engineering bedrock are assumed to be $Vs = 144$ m/s and $\gamma = 2.0E+04N/m^3$, which are needed for the soil dynamic analyses later.

As recommended in Ishihara (2010), the structural integrity and safety of wind turbine support structures are required against the level II earthquake with a recurrence period of 500 years. This also fulfills the requirement of the IEC 61400-1 guideline which states that the ground acceleration corresponding to a 475-year recurrence period should be

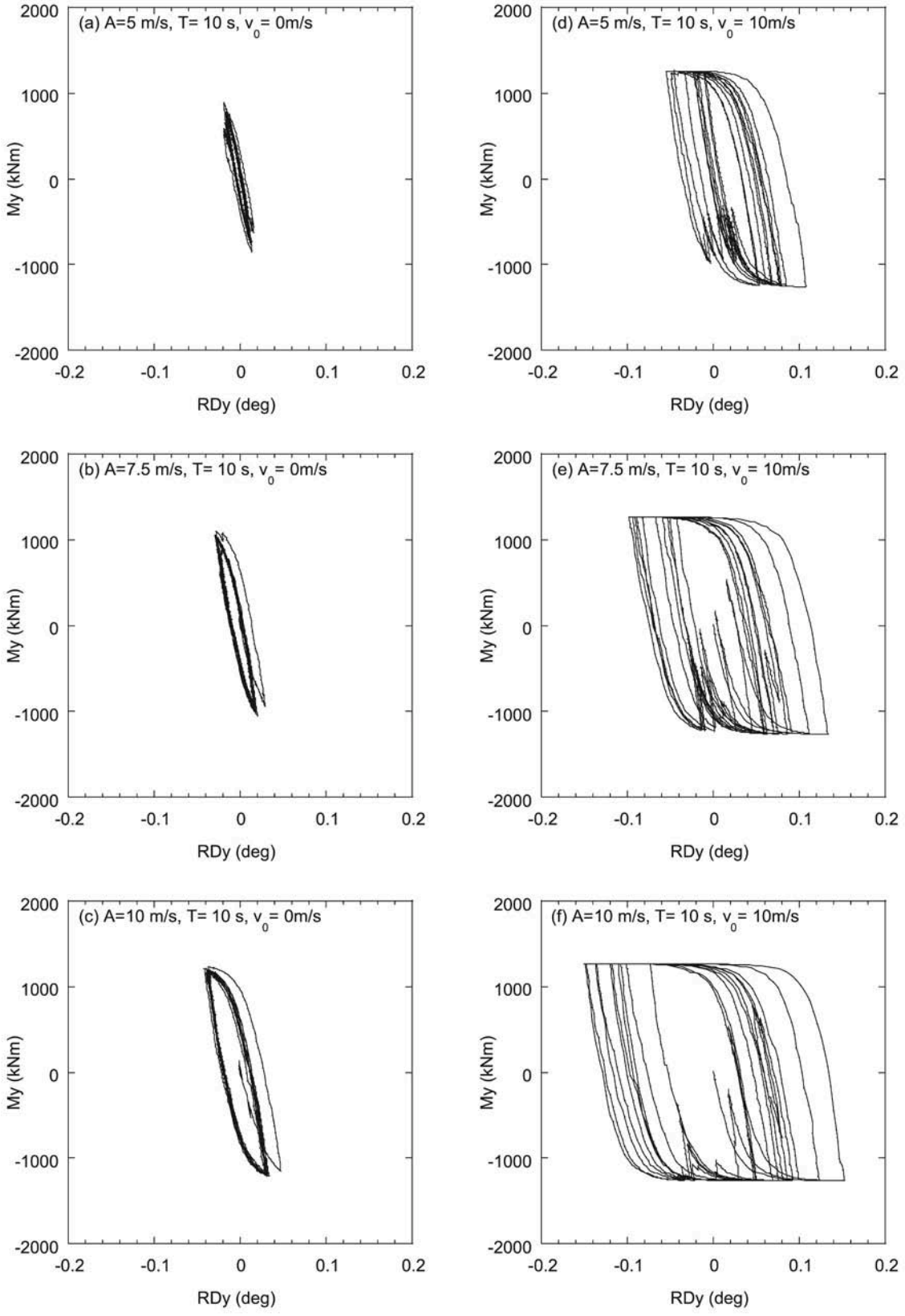

Fig. 8. Hysteretic response for the $M_y - \theta_y$ spring at 1 m below the mudline.

Table 6
Parameters for the emergency stop.

Item	Value
Wind condition	Wind speed from 11.4 m/s to 0 m/s
Seismic condition	15 artificial Level II earthquake waves
Misalignment between wind and earthquake	0 deg; 45 deg; 90 deg
Nacelle acceleration limit	300gal
Pitch feathering rate	8 deg/s

Table 7
Monopile parameters.

Foundation type	Diameter (m)	Thickness (m)	Embedment (m)
Monopile	6	0.06	36

Table 8
Uniform sand properties used in this section.

Soil properties	G_r (MPa)	B_r (MPa)	c_u (kPa)	φ (deg)	γ' (kN/m3)
Sand	41.5	90.0	0.0	39.5	9.81

Note: G_r, low-strain shear modulus; B_r, low-strain bulk modulus; c_u, cohesion; φ, soil friction angle; γ', effective unit weight.

considered for the seismic response evaluation of a wind turbine. For the level II earthquake, the response spectrum at the engineering bedrock is defined as follows:

$$S_{a_0}(T,0.05)=\begin{cases} a_0(1+9.375T) & (0\le T\le 0.16) \\ 2.5a_0 & (0.16<T<0.64) \\ 1.6a_0/T & (T\ge 0.64) \end{cases} \quad (22)$$

where $S_{a_0}(T,0.05)$ specifies the basic peak ground acceleration a_0 at the engineering bedrock along with the frequency characteristic of the ground motions. a_0 is 3.2 m/s^2 for the level II earthquake and 1.6 m/s^2 for the level I earthquake; T is the natural period (s). In this study, a 120-s seismic time history is generated based on the target spectrum described above, in which the phase characteristics of 4 typical real earthquake waves such as El Centro NS, Taft NS, Hachinohe EW, and JMA Kobe EW and 11 random phase properties are used. Fig. 9 shows the response spectrum of the generated earthquake wave with a damping ratio of 5%. Since the generated seismic waves are specified at the engineering bedrock, a series of site response analyses are performed in SHAKE to obtain the seismic waves at different elevations. Fig. 10 illustrates the time histories of seismic waves at typical elevations generated by a level II earthquake with the phase of El Centro NS. It is noticed that the seismic wave becomes stronger along with the decrease of elevation depth.

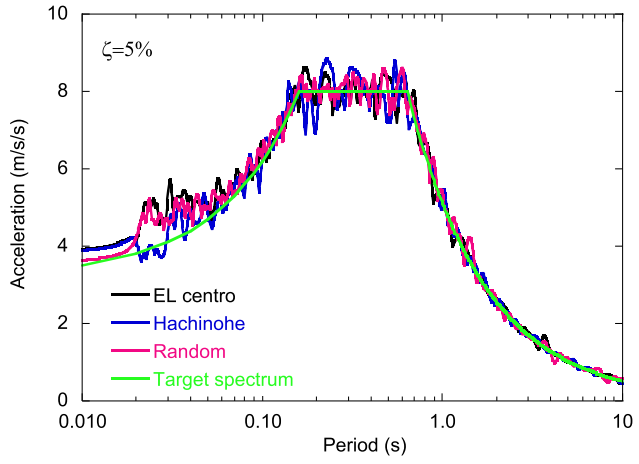

Fig. 9. Response spectrum of the generated level II seismic wave with the damping ratio of 5%.

As portrayed in Fig. 11, three misalignment levels of wind and earthquake (0 deg, 45 deg, and 90 deg) are investigated to illustrate the effects of the misalignment of wind and earthquake. Larger misalignments are not considered since they would reduce the dynamic responses of the monopile-supported wind turbine. To model the soil-monopile interaction properly, the spring interval of 1m is used for the depth range of (-20m, -25m) while the spring interval of 2m is used for the depth range of (-25m, -50m). It is important to note the damping used in this study. Each of the simulations has a duration of 121s and a time step of 0.0005s. The emergency stops are triggered when the acceleration of the nacelle reaches 300 gals. Once it is triggered, the blades are turned to pitch feathering with a rate of 8 deg/s.

4.2. Results and discussion

Fig. 12 illustrates various time histories during the emergency stop with the nacelle acceleration limit of 300 gals and the pitch feathering rate of 8° per second for the 0-degree misalignment. More specifically, Fig. 12(a) depicts the time histories of wind velocity and seismic acceleration. A uniform wind with the rated velocity of 11.4 m/s is adopted since the turbulent component is less important to the extreme load compared to the mean component. Fig. 12(b) shows the time histories of the resultant nacelle acceleration of X and Y directions. That is why the value is no less than 0 gal. It is noticed that the nacelle acceleration limit reaches 300 gals at 10s, from which the emergency stop starts by feathering the blade pitch at the rate of 8° per second. As shown in Fig. 12(c), the blade pitch angle keeps 0° until 10s and increases linearly to 90° at the interval of 21.25s, at which the emergency stop is finished and after which the blade is feathered and the pitch angle does not change any more. It is interesting to note that the rotor speed experiences a short increase before it decreases sharply and it takes more time for the rotor speed reduces to zero than that for the pitch angle reaches 90°. Fig. 12(d) portrays the corresponding time histories of the tower base moment in the X direction for the misalignments of 0-degree and 90-degree, while Fig. 12(e) presents those in the Y direction. For the 0-degree misalignment, it is found although the amplitude of seismic wave decreases after the 50s, the moment for the X direction (My) increases after the 50s. This is because after the emergency stop occurs, the X-direction aerodynamic damping reduces to near zero. The loss of aerodynamic damping causes the increase of moment. By comparing the moments of the X and Y directions for the 90-degree misalignment, it is known that the aerodynamic load (My) is much smaller than the seismic load (Mx), which means that the earthquake excitation is the design driving load, prevailing over the wind excitation for the design of wind turbine support structures.

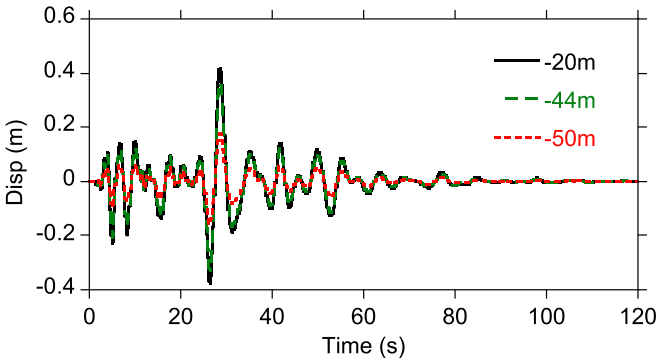

Fig. 10. Time histories of displacements at different elevations.

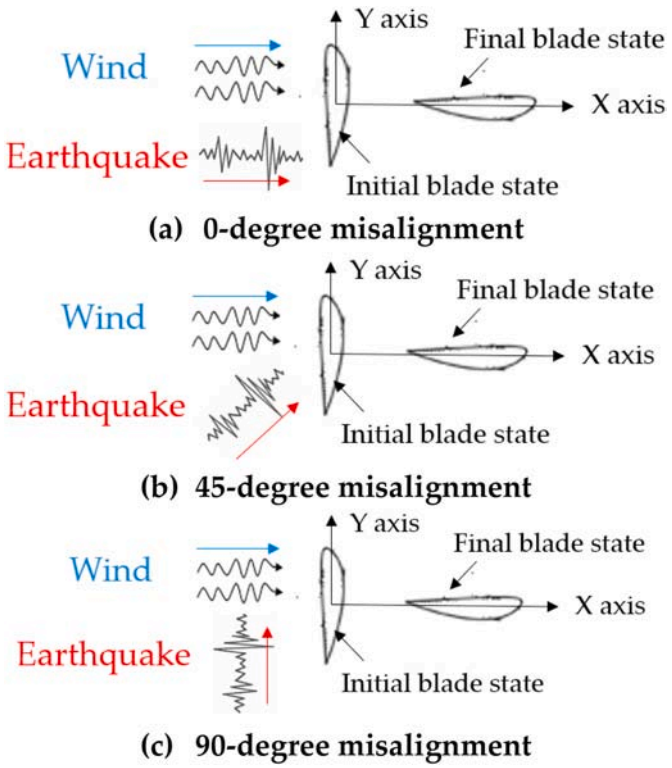

Fig. 11. The misalignment configuration of wind and earthquake.

To obtain the distribution of seismic loading along the tower, the maximum combined seismic and aerodynamic loads of 15 seismic waves are averaged for each misalignment and presented in Fig. 13. It is found that due to the nonlinearity of soil-structure interaction and the characteristics of seismic waves, the shear force and bending moment are not linearly distributed along the tower, which is different from the predictions using the fixed foundation. In addition, the misalignment affects the combined seismic and aerodynamic loads largely. The 0-degree misalignment outputs the maximum bending moment, the 45-degree misalignment shows the middle value, while the 90-degree misalignment yields the smallest one, from which it is concluded that the bending moment of tower decreases along with the increase of the misalignment of wind and earthquake.

5. Conclusion and future research subject

In this study, a new FounDyn module is created in OpenFAST to consider foundation dynamics based on a site-specific soil reaction framework. The site-specific soil reaction framework has the same configuration of the semi-analytical 1D model proposed by Wang and Ishihara, 2022a to consider effects of plie diameter and aspect ratio but uses new site-specific soil reaction models. The soil reaction models are nonlinear and hysteretic, which match the desired modulus reduction curve by identifying three parameters in a hyperbolic function and a linear function using genetic algorithm (GA) and manual parameter tuning algorithm, and the desired damping curve by applying the Ishihara-Yoshida rule that controls the unloading-reloading curves iteratively through three parameters.

The FounDyn module is created in OpenFAST to consider the foundation dynamics using the proposed site-specific soil reaction framework. The FounDyn module receives the motions from the SubDyn module and sends the forces back to the SubDyn module. The FounDyn module is verified by the well-confined OC3 project in terms of modal frequencies, tower top displacement and shear force and moment at the mudline, and reasonable agreement is achieved between them. Driven

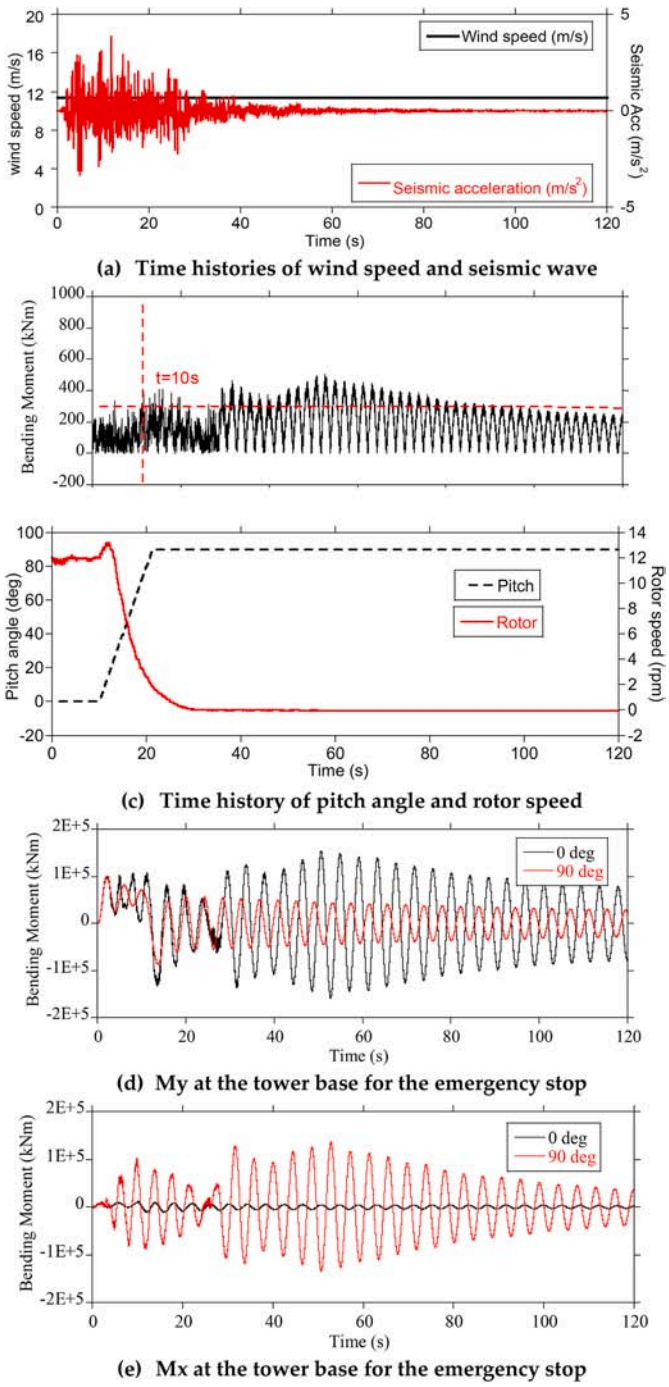

Fig. 12. Illustrations of various time histories during the emergency stop.

by the OpenFAST plus FounDyn module, the integrated dynamic analysis of monopile supported wind turbines can be conducted considering the aerodynamics, hydrodynamics, aeroelasticity, servo dynamics and foundation dynamics, which means the FounDyn module is an appealing supplement to the current version of OpenFAST.

The application of FounDyn module is demonstrated to perform dynamic responses of a NREL 5 MW monopile supported wind turbine under coupled wind and earthquake. Considering the fact that emergency shutdown is the least known operational scenario, a series of emergency shutdown analyses are performed in which the misalignment of wind and wave is considered. The results show that the misalignment of wind and wave affects the bending moments of tower significantly. The earthquake excitation is found to be the design driving load,

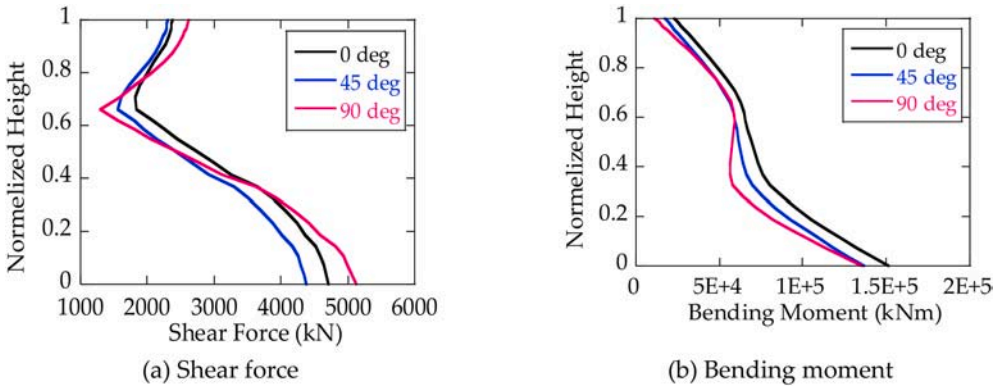

Fig. 13. Profiles of maximum combined loads for the emergency stop with various angles between wind and earthquake.

prevailing over the wind excitation for the design of wind turbine supporting structures.

It is believed that the FounDyn module is a meaningful improvement for the coupled analyses of offshore wind turbines. However, it suffers to some limitations when it is applied to design offshore wind turbines. Some examples of future research subjects are as follows:

1. During the implementation of the Ishihara-Yoshida rule to match the damping curve in the proposed model, the bisection method is used to iterate the damping parameters A, B, E, which is unconditionally stable, but less efficient. It is necessary to implement other more advanced algorithms (i.e., Ridders' Method, Ridders, 1979) to improve the simulation efficiency, especially when the proposed model is coupled with the OpenFAST program.
2. The current soil reaction framework contains 8 types of soil reactions that are distributed along the whole pile shaft and base. The complicated model configuration reduces the stability and efficiency of simulations when it is coupled with the OpenFAST program, i.e., the time increment usually shall be small enough to obtain the stable results. This inconvenience can be addressed by the recently proposed mechanism-based family of "p-y+M-theta" models (Wang et al., 2020; Lai et al., 2021), which unify the predictions for interactions between soil and piles covering a wide range of rigidity and geometry (i.e., flexible, semi-rigid and rigid piles) using a single set of parameters. The physical soundness of the model lies in the new understanding associated with three-zones of failure mechanisms around a laterally loaded pile, which were firstly discovered by Hong et al., 2017 based on 'visualized' half-pile centrifuge model tests and numerical analyses using an advanced cyclic model.
3. The current site-specific soil reaction framework is mainly proposed for seismic analyses of wind turbines. Therefore, it can be further improved for wind and wave analyses of wind turbines by incorporating the cyclic effect into the site-specific soil reaction framework.
4. Although the site-specific soil reaction framework suits for all types of pile foundations, i.e., monopile, jacket, pile group, etc., the current version of the FounDyn module considers the monopile foundation only. In the future, other pile foundations and other types of foundations (i.e., gravity foundation, monopod, tripod, etc.) shall be considered in the FounDyn module.
5. Since the FounDyn module is evaluated by a limited number of numerical analyses in this study, it shall be verified or validated by more numerical analyses, experiments or field tests before it is widely-used for the design of offshore wind turbines.

CRediT authorship contribution statement

Lilin Wang: Conceptualization, Methodology, Software, Data curation, Writing – original draft, Visualization, Investigation, Validation. **Takeshi Ishihara:** Methodology, Supervision, Writing – review & editing.

Declaration of competing interest

The authors declare that they have no known competing financial interests or personal relationships that could have appeared to influence the work reported in this paper.

Data availability

No data was used for the research described in the article.

Acknowledgement

The authors express his deepest gratitude to Dr. Jason Jonkman and Dr. Andy Platt in National Renewable Energy Laboratory (NREL) for sharing the method to implement a new module in OpenFAST.

Appendix

Appendix A. The input parameters in the proposed model

The simple way to determine the ultimate capacity and representative displacement for the proposed model can be found in Eq. (A1)-(A10). More information can be found in Wang and Ishihara (2022a).

$$p_{ult}(z) = \left(\frac{\pi}{4} + \frac{1}{3}\tan\delta\right) D\sigma_{r0} + \frac{\pi}{4} cD \tag{A1}$$

$$y_{50}(z) = \frac{p_{ult}(z)}{K_{p_y}(z)} \tag{A2}$$

Here, $\sigma_{r0} = \kappa(2c\sqrt{K_p} + \gamma' z K_p), K_p = \tan^2\left(45^\circ + \frac{\varphi}{2}\right), \kappa = \begin{cases} 6.612 \cdot D^{-0.469} & \text{for sand} \\ \min(2.714 \cdot D^{1.112}, \ 2.2) & \text{for clay} \end{cases}, \delta = \left(\frac{1}{3} \sim \frac{2}{3}\right)\varphi, K_{p_y} = \frac{0.65E_s}{1-\nu_s^2}\sqrt[12]{\frac{E_s D^4}{E_p I_p}}, E_s = 2(1+\upsilon_s)G_s, I_p = \frac{\pi}{64}[D^4 - (D-2t)^4]$

$$Q_{ult,\mathrm{pb}} = \eta\left(cN_c F_{cs} F_{cd} F_{ci} + \gamma' D_f N_q F_{qs} F_{qd} F_{qi} + 0.5\gamma' B N_\gamma F_{\gamma s} F_{\gamma d} F_{ri}\right)\frac{\pi D^2}{4} \tag{A3}$$

$$z_{50,\mathrm{pb}} = \frac{Q_{ult,\mathrm{pb}}}{K_{Q_{z,\mathrm{pb}}}} \tag{A4}$$

Here, $K_{Q_{z,\mathrm{pb}}} = \frac{GL}{1-\upsilon}\left[0.73 + 1.54\left(\frac{D}{L}\right)^{0.75}\right]$

$$M_{ult,\mathrm{pb}} = \frac{1}{2} \cdot N_{\mathrm{pb}}\left(1 - \frac{N_{\mathrm{pb}}}{Q_{ult,\mathrm{pb}}}\right)D_2 \tag{A5}$$

$$\theta_{50,\mathrm{pb}} = \frac{M_{ult,\mathrm{pb}}}{K_{M_{x,\mathrm{pb}}}} \tag{A6}$$

Here, $K_{M_{x,\mathrm{pb}}} = \frac{G_s D^3}{3(1-\upsilon_s)}, A = \frac{\pi}{4}D^2, D_2 = \sqrt{A}$

$$t_{ult}(z) = (k_0 \gamma' z \tan\delta + k_1 c)\pi D \tag{A7}$$

$$z_{50}(z) = \frac{t_{ult}(z)}{K_{t_z}} \tag{A8}$$

Here, $K_{t_z} = \left(\frac{6.8}{\pi}\left(\frac{L}{D}\right)^{-1.71}E_s\right)\pi D$

$$M_{ult}(z) = \frac{1}{2}cD^2 + \frac{\pi}{8}D^2 \tan\delta\sigma_{r0} \tag{A9}$$

$$\theta_{50}(z) = \frac{M_{ult}(z)}{K_{M_x}} \tag{A10}$$

Here, $K_{M_x} = 0.85\left(\frac{L}{D}\right)^{-1.71}E_s L^2$

$$S_{ult,\mathrm{pb}} = \left(c\frac{\pi}{4}D^2 + N_{\mathrm{pb}} \tan\delta\right) \tag{A11}$$

$$y_{50,\mathrm{pb}} = \frac{S_{ult,\mathrm{pb}}}{K_{S_{y,\mathrm{pb}}}} \tag{A12}$$

Here, $K_{S_{y,\mathrm{pb}}} = \frac{4G_s D}{(2-\upsilon_s)}, N_{\mathrm{pb}} = N_0 - \min\left(\frac{\sum_{z=0}^{L} K_{tz}}{\sum_{z=0}^{L} K_{tz} + K_{Q_{z,\ \mathrm{pb}}}} N_0, \ \sum_{z=0}^{L} t_{ult}(z)\right), k_0 = 0.4, k_1 = 0.5,$

where c is cohesion of soil, γ' is the effective unit weight of soil, φ is the friction angle of soil, D_r is the relative density of soil, P_a is the atmospheric pressure. N_c, N_q and N_γ are the bearing capacity factors, F_{cs}, F_{qs} and $F_{\gamma s}$ are the shape factors, F_{cd}, F_{qd} and $F_{\gamma d}$ are the depth factors, F_{ci}, F_{qi} and F_{ri} are the inclination factors, which can be found in Meyerhof (1963). η is the plugging coefficient. In the Chinese method (Chinese Department of Construction, 2008), $\eta = 1$ for closed-ended piles, $\eta = 0.16z/D$ when $z/D < 5$, and $\eta = 0.8$ when $z/D \geq 5$. In the FinnRA method (FinnRA, 2000), $\eta = 0.8$ for sandy soil if $z/D = 15$, and the value decreases linearly with the z/D ratio. G_s and υ_s are the shear modulus and Poisson ratio of soil, respectively. t and E_p are the thickness and Young's modulus of monopile, respectively.

References

Bush, E., Manuel, L., 2009. Foundation Models for Offshore Wind Turbines, Aerospace Sciences Meetings. American Institute of Aeronautics and Astronautics. https://doi.org/10.2514/6.2009-1037.

Chinese Department of Construction, 2008. JGJ 94-2008: Technical code for building pile foundations. (In Chinese).

FinnRA, 2000. Steel Pipe Piles, Helsinki.

Hardin, B.O., Drnevich, V.P., 1972. Shear modulus and damping in soils: design equations and curves. J. Soil Mech. Found Div. 98 (7), 667–692.

Hong, Y., He, B., Wang, L.Z., Wang, Z., Ng, C.W.W., Mašín, D., 2017. Cyclic lateral response and failure mechanisms of a semi-rigid pile in soft clay: centrifuge tests and numerical modeling. Can. Geotech. J. 54, 806–824.

IEC 61400-1, 2019. Wind Turbines – Part 1: Design Requirements, Ed, p. 4.

Ishihara, T., 2010. Guidelines for Design of Wind Turbine Support Structures and Foundations (In Japanese).

Ishihara, K., Yoshida, N., Tsujino, S., 1985. Modelling of stress-strain relations of soils in cyclic loading. In: International Conference on Numerical Methods in Geomechanics, pp. 373–380.

Jonkman, J.M., Buhl, M.L., 2005. FAST User's Guide. National Renewable Energy Laboratory.

Jonkman, J.M., Musial, W., 2010. Offshore Code Comparison Collaboration (OC3) for IEA Task 23 Offshore Wind Technology and Deployment. Technical Report NREL/TP-5000–48191.
Jonkman, J.M., Butterfield, S., Passon, P., Larsen, T., Camp, T., Nichols, J., Azcona, J., Martinez, A., 2008. Offshore code comparison collaboration within IEA wind annex XXIII: phase II results regarding monopile foundation modeling. Technical report no. NREL/CP-500- 47534.
Jung, S., Kim, S.R., Patil, A., Hung, L.C., 2015. Effect of monopile foundation modeling on the structural response of a 5-MW offshore wind turbine tower[J]. Ocean Eng. 109, 479–488.
Kim, B., Jin, J., Bitkina, O., Kang, K., 2016. Ultimate load characteristics of NREL 5-MW offshore wind turbines with different substructures[J]. Int. J. Energy Res. 40, 639–650.
Krathe, V.L., 2015. Aero-hydro Dynamic Analysis of Offshore Wind Turbine - Implementation of Nonlinear Soil-Structure Interaction in Software fast[D], vol. 2015. Msc Thesis.
Krathe, V.L., Kaynia, A.M., 2017. Implementation of a non-linear foundation model for soil-structure interaction analysis of offshore wind turbines in FAST[J]. Wind Energy 20 (4), 695–712.
Lai, Y., Wang, L., Zhang, Y., Hong, Y., 2021. Site-specific soil reaction model for monopiles in soft clay based on laboratory element stress-strain curves. Ocean Eng. 220, 108437.
Loken, I.B., Kaynia, A.M., 2019. Effect of foundation type and modelling on dynamic response of offshore wind turbines[J]. Wind Energy 22 (12), 1667–1683.
Meyerhof, G.G., 1963. Some recent research on the bearing capacity of foundations. Can. Geotech. J. 1 (1), 16–26.
Prowell, I., 2011. An Experimental and Numerical Study of Wind Turbine Seismic Behavior. University of California, San Diego.
Ridders, C.J.F., 1979. A new algorithm for computing a single root of a real continuous function. IEEE Trans. Circ. Syst. 979–980.
Wang, L., Ishihara, T., 2020. A study of the effects of foundation uplift on the seismic loading of wind turbine tower and shallow foundation using a new dynamic Winkler model. Eng. Struct. 219, 110745.
Wang, L., Ishihara, T., 2022a. A semi-analytical one-dimensional model for offshore pile foundations considering effects of pile diameter and aspect ratio. Ocean Eng. 250, 110874.
Wang, L., Ishihara, T., 2022b. New p-y model for seismic loading prediction of pile foundations in non-liquefiable and liquefiable soils considering modulus reduction and damping curves. Soils Found. 62 (2022), 101201.
Wang, L., Lai, Y., Hong, Y., Mašín, D., 2020. A unified lateral soil reaction model for monopiles in soft clay considering various length-to-diameter (L/D) ratios. Ocean Engineering 212, 107492.
Wei, S., Hyun-chul, P., Chin-hwa, C., Jae-ha, B., Youngchan, K., Chang-wan, K., 2013. Load analysis and comparison of different jacket foundations[J]. Renew. Energy 54, 201–210.
Yang, Y., Bashir, M., Li, C., Michailides, C., Wang, J., 2020. Mitigation of coupled wind-wave-earthquake responses of a 10 MW fixed-bottom offshore wind turbine. Renew. Energy 157, 1171–1184.
Zhang, Y., Aamodt, K.K., Kaynia, A.M., 2021. Hysteretic damping model for laterally loaded piles. Mar. Struct. 76, 102896.